AIAA JOURNAL
Vol. 48, No. 4, April 2010

Consistent Regularization for Damage Detection with Noise and Model Errors

X. Y. Li* and S. S. Law†
Hong Kong Polytechnic University, Kowloon, Hong Kong, People's Republic of China

DOI: 10.2514/1.43322

Two techniques are proposed in a new regularization method for the inverse identification of local damages in a structure. One technique is the introduction of a new side condition, and the other technique restricts the range of variation of the regularization parameter by consistently choosing the optimal point on the *L*-curve. Both techniques fully make use of the information from results obtained in previous iteration steps. A plane frame structure is studied with two damaged elements and different levels of noise and model errors. Numerical results show that the proposed consistent regularization method is very effective at improving the results of the ill-conditioned inverse-problem phenomenon, compared with the Tikhonov regularization.

Introduction

A NUMBER of methods have been developed for damage detection in the last two decades. Many of the methods are based on the observation of dynamic behavior of a structure (Doebling et al. [1], Brincker et al. [2], Maeck and DeRoeck [3]), among which the sensitivity approach via a model-updating technique is commonly accepted and applied extensively in the engineering industry because of its clear mathematical background and quantitative indications. However, this type of method is weak at accommodating the influence of measurement errors, leading to ill-conditioned problems, as demonstrated by Friswell et al. [4] and Humar et al. [5]. This shortcoming means that the existence and uniqueness of the solution is not ensured and numerical instability is likely to take place in the course of the solution process [6,7].

Investigations have since been conducted to deal with the ill-conditioned problems in model updating. Hansen [8,9] and Vogel [10] proposed regularization methods for obtaining a solution of the inverse problem. It is recognized in regularization theory that the conventional output error, which is usually the vector of differences between the computed and measured responses, can be made unrealistically small if the process of damage identification is allowed to behave badly, such that the variable has arbitrarily large deviations from the true set of parameter change, or there may be infinite sets of ill-posed solutions. A stable solution scheme can be achieved by imposing certain constraints in the form of added penalty terms with adjustable weighting parameters based on posterior knowledge.

Recently, Titurus and Friswell [11] presented the sensitivity-based model-updating method with an additional regularization criterion and computed the solutions based on the generalized singular value decomposition. Specific features of the parameter and response paths were explored when the regularization parameter varies. The four different types of spaces that arise in the solution were discussed, together with the characteristics of the families of the regularized solution. Weber et al. [12] applied the Tikhonov regularization and truncated singular value decomposition consistently to a nonlinear updating problem. Line-search and stopping criteria known from numerical optimization were adapted to the regularized problem. The optimal regularization parameter was determined by generalized cross-validation.

From experiences gained in model updating with laboratory test structures, the authors found that Tikhonov regularization can give the optimal solution when there is no noise or very small noise in the measurement. But in the updating procedure for a nonlinear inverse problem with the inclusion of noise and model error, the signal-to-noise ratio is getting smaller [13,14] with each iteration, and the solution obtained from a poor regularization parameter is usually unacceptable. The algorithm does not accurately converge, and the results depend strongly on the convergence criteria and tolerances.

In this paper, two techniques are proposed in a new regularization method for the identification of local damages in a structure. One technique proposed a new side condition that classified the elements as possibly damaged and undamaged elements, which will be treated differently later. The other technique restricts the range of variation of the regularization parameter, such that the regularization solution will be in a realistic range, and the correct optimal point from the curvature of the *L*-curve is consistently chosen to ensure a continuous converging process. Both techniques make full use of the information from results obtained in previous iteration steps. A plane frame structure is studied with two damaged elements and different levels of noise and model errors to illustrate the application of the proposed method. Numerical results show that the proposed consistent regularization method is very effective at improving the results in the inverse problem with ill-conditioning, compared with the conventional Tikhonov regularization.

Formulation

Damage-Detection Method

A time-domain approach of model improvement is adopted [13] in which the unit impulse response function (IRF) is used to detect local damage in the following studies. The time-domain approach has a benefit over the conventional frequency-domain approach, that there is a large amount of redundant measured information limited only by the time of measurement. The measured response is decomposed into wavelets for the analysis, because the discretized wavelet transform approach is generally applicable to responses from different types of excitation. The IRF also has the advantage that it can be measured repeatedly.

Sensitivity Matrix of Impulse-Response-Function Wavelet Coefficient

The equation of motion of an N-degree-of-freedom (DOF) damped structural system under the unit impulse excitation can be converted to [13]

$$\begin{cases} \mathbf{M}\ddot{\mathbf{h}}(t) + \mathbf{C}\dot{\mathbf{h}}(t) + \mathbf{K}\mathbf{h}(t) = 0 \\ \mathbf{h}(0) = 0,\ \dot{\mathbf{h}}(0) = \mathbf{M}^{-1}\mathbf{D} \end{cases} \tag{1}$$

Received 20 Jan. 2009; revision received 3 Aug. 2009; accepted for publication 6 Sept. 2009.

*Postdoctoral Research Fellow, Civil and Structural Engineering Department, Hung Hom.

†Associate Professor, Civil and Structural Engineering Department, Hung Hom.

where $\mathbf{M}$, $\mathbf{C}$, and $\mathbf{K}$ are the $N \times N$ mass, damping, and stiffness matrices, respectively; $\mathbf{D}$ is the mapping matrix relating the force excitation location to the corresponding DOF of the system; and $\ddot{\mathbf{h}}(t)$ is the unit impulse acceleration vector. The system is assumed to be in static equilibrium before the application of the unit impulse excitation.

An approximate model is adopted in which the local damage in the structural system is expressed as

$$\Delta\mathbf{K} = \sum_{i=1}^{\text{ne}} \Delta\alpha_i \mathbf{K}_i$$

where $\Delta\alpha_i$ is a fractional change in the stiffness of an element with $-1.0 \le \Delta\alpha_i \le 0.0$, ne is the number of elements in the structure, and $\mathbf{K}_i$ is the ith elemental stiffness matrix. The global stiffness matrix for the damaged structure becomes $\mathbf{K} + \Delta\mathbf{K}$.

Differentiate Eq. (1) with respect to the structural parameter α_i and using Newmark method [15] and discrete wavelet transform (DWT). The sensitivity $\partial\ddot{\mathbf{h}}^{\text{DWT}}/\partial\alpha$ can then be obtained [13]. The sensitivity matrix can then be written as

$$\mathbf{S} = \begin{bmatrix} \frac{\partial \ddot{\mathbf{h}}_l^{\text{DWT}}(t_1)}{\partial\alpha_1} & \frac{\partial \ddot{\mathbf{h}}_l^{\text{DWT}}(t_1)}{\partial\alpha_2} & \cdots & \frac{\partial \ddot{\mathbf{h}}_l^{\text{DWT}}(t_1)}{\partial\alpha_m} \\ \frac{\partial \ddot{\mathbf{h}}_l^{\text{DWT}}(t_2)}{\partial\alpha_1} & \frac{\partial \ddot{\mathbf{h}}_l^{\text{DWT}}(t_2)}{\partial\alpha_2} & \cdots & \frac{\partial \ddot{\mathbf{h}}_l^{\text{DWT}}(t_2)}{\partial\alpha_m} \\ \vdots & \vdots & \vdots & \vdots \\ \frac{\partial \ddot{\mathbf{h}}_l^{\text{DWT}}(t_{\text{nt}})}{\partial\alpha_1} & \frac{\partial \ddot{\mathbf{h}}_l^{\text{DWT}}(t_{\text{nt}})}{\partial\alpha_2} & \cdots & \frac{\partial \ddot{\mathbf{h}}_l^{\text{DWT}}(t_{\text{nt}})}{\partial\alpha_m} \end{bmatrix} \tag{2}$$

where l refers to the lth DOF (sensor location) of the structure, matrix $\mathbf{S}$ is also a function of time, and m is the number of structural parameters to be identified with $m \le \text{ne}$, in general. But $m = \text{ne}$ is adopted in the present study, and nt is the number of data points used. A Daubechies wavelet is selected, as it satisfies the two crucial requirements: the orthogonality of local basis functions and second-order accuracy or higher, depending on the dilation expression adopted.

Impulse-Response-Function Wavelet Coefficient

The measured response provides $\ddot{\mathbf{h}}_l^{\text{DWT}}$ [13]. The equation of motion of the structure under general excitation is

$$\mathbf{M}\,\ddot{\mathbf{x}}(\mathbf{t}) + \mathbf{C}\dot{\mathbf{x}}(\mathbf{t}) + \mathbf{K}\mathbf{x}(\mathbf{t}) = \mathbf{D}\cdot\mathbf{F}(\mathbf{t}) \tag{3}$$

where $\mathbf{F(t)}$ is the vector of excitation force. If the system has zero initial conditions, the acceleration response $\ddot{\mathbf{x}}_l(t_n)$ from location l at time t_n is

$$\ddot{\mathbf{x}}_l(t_n) = \int_0^{t_n} \ddot{\mathbf{h}}_l(\tau)\cdot\mathbf{F}(t_n - \tau)\,\mathrm{d}\tau \tag{4}$$

Applying DWT to $\ddot{\mathbf{h}}_l(\tau)$ and $\mathbf{F}(t_n - \tau)$, respectively, and using the orthogonal property of the wavelet basis [13], the acceleration vector $\ddot{\mathbf{x}}_l$ can be written in matrix form as

$$\ddot{\mathbf{x}}_l = \mathbf{F}^{\text{DWT}}\cdot\ddot{\mathbf{h}}_l^{\text{DWT}} \tag{5}$$

where

$$\ddot{\mathbf{x}}_l = [\,\ddot{\mathbf{x}}_l(t_1) \quad \ddot{\mathbf{x}}_l(t_2) \quad \cdots \quad \ddot{\mathbf{x}}_l(t_{\text{nt}})\,]^T,$$

$$\ddot{\mathbf{h}}_l^{\text{DWT}} = [\,\ddot{\mathbf{h}}_{l,0}^{\text{DWT}} \quad \ddot{\mathbf{h}}_{l,1}^{\text{DWT}} \quad \cdots \quad \ddot{\mathbf{h}}_{l,2^j+k}^{\text{DWT}}\,]^T,$$

$$\mathbf{F}^{\text{DWT}} = \begin{bmatrix} \mathbf{F}_0^{\text{DWT}}(t_1) & \mathbf{F}_1^{\text{DWT}}(t_1) & \cdots & \mathbf{F}_{2^j+k}^{\text{DWT}}(t_1)/2^j \\ \mathbf{F}_0^{\text{DWT}}(t_2) & \mathbf{F}_1^{\text{DWT}}(t_2) & \cdots & \mathbf{F}_{2^j+k}^{\text{DWT}}(t_2)/2^j \\ \vdots & \vdots & \vdots & \vdots \\ \mathbf{F}_0^{\text{DWT}}(t_{\text{nt}}) & \mathbf{F}_1^{\text{DWT}}(t_{\text{nt}}) & \cdots & \mathbf{F}_{2^j+k}^{\text{DWT}}(t_{\text{nt}})/2^j \end{bmatrix}$$

and $\ddot{\mathbf{h}}_l^{\text{DWT}}$ in Eq. (5) can be expressed in the form of a pseudoinverse as

$$\ddot{\mathbf{h}}_l^{\text{DWT}} = (\mathbf{F}^{\text{DWT}^T}\cdot\mathbf{F}^{\text{DWT}})^{-1}\cdot\mathbf{F}^{\text{DWT}^T}\cdot\ddot{\mathbf{x}}_l \tag{6}$$

Identification Equation and Implementation Procedure

Because the relationship between the impulse-response-function wavelet coefficient $\ddot{\mathbf{h}}_l^{\text{DWT}}$ and the fractional stiffness parameter $\boldsymbol{\alpha}$ is nonlinear, a nonlinear model-updating technique such as the Gauss–Newton method is required. This kind of method has the advantage that the second derivatives, which can be challenging to compute, are not required. The Gauss–Newton method in the damage-detection procedure can be described in terms of the wavelet coefficient $\ddot{\mathbf{h}}_l^{\text{DWT}}$ at the lth DOF of the structure as

$$\ddot{\mathbf{h}}_l^{\text{DWT}}(\boldsymbol{\alpha}^d) = \ddot{\mathbf{h}}_l^{\text{DWT}}(\boldsymbol{\alpha}^0) + \mathbf{S}(\boldsymbol{\alpha}^0)\cdot\boldsymbol{\Delta\alpha}^1 + \mathbf{S}(\boldsymbol{\alpha}^0 + \boldsymbol{\Delta\alpha}^1)\cdot\boldsymbol{\Delta\alpha}^2 + \cdots \tag{7}$$

The superscripts 0, 1, and 2 denote the iteration number, and d denotes the damaged state. The damage identification equation for the $(k+1)$th iteration is

$$\mathbf{S}_k\cdot\boldsymbol{\Delta\alpha}^{k+1} = (\boldsymbol{\Delta}\ddot{\mathbf{h}}_l^{\text{DWT}})_k, \qquad (k = 0, 1, 2, \ldots) \tag{8}$$

The iteration in Eq. (8) starts with an initial value $\boldsymbol{\alpha}^0$, leading to

$$(\boldsymbol{\Delta}\ddot{\mathbf{h}}_l^{\text{DWT}})_0 = \ddot{\mathbf{h}}_l^{\text{DWT}}(\boldsymbol{\alpha}^d) - \ddot{\mathbf{h}}_l^{\text{DWT}}(\boldsymbol{\alpha}^0)$$

and $\mathbf{S}_0 = \mathbf{S}(\boldsymbol{\alpha}^0)$. The parameter vector

$$\boldsymbol{\alpha}^k = \boldsymbol{\alpha}^0 + \sum_{i=1}^{k} \boldsymbol{\Delta\alpha}^i$$

the sensitivity matrix $\mathbf{S}_k = \mathbf{S}(\boldsymbol{\alpha}^k)$, and the residual vector

$$(\boldsymbol{\Delta}\ddot{\mathbf{h}}_l^{\text{DWT}})_k = \ddot{\mathbf{h}}_l^{\text{DWT}}(\boldsymbol{\alpha}^d) - \ddot{\mathbf{h}}_l^{\text{DWT}}(\boldsymbol{\alpha}^0) - \sum_{i=0}^{k-1} \mathbf{S}_i\boldsymbol{\Delta\alpha}^{i+1}$$

$(k = 1, 2, \ldots)$ of the next iteration is then computed from results in the previous iterations.

Vectors of the impulse-response-function wavelet coefficient at the lth DOF of the damaged and intact states are $\ddot{\mathbf{h}}_l^{\text{DWT}}(\boldsymbol{\alpha}^d)$ and $\ddot{\mathbf{h}}_l^{\text{DWT}}(\boldsymbol{\alpha}^0)$, respectively. The vector $\ddot{\mathbf{h}}_l^{\text{DWT}}(\boldsymbol{\alpha}^0)$ from the physical intact structure is computed, in general, from the associated analytical model via dynamic analysis, and $\ddot{\mathbf{h}}_l^{\text{DWT}}(\boldsymbol{\alpha}^d)$ is obtained by Eq. (6) from the damaged structure from measurement.

The iteration is terminated when a preselected criterion is met. The final identified damage vector becomes

$$\Delta\boldsymbol{\alpha} = \Delta\boldsymbol{\alpha}^1 + \Delta\boldsymbol{\alpha}^2 + \cdots + \Delta\boldsymbol{\alpha}^n \tag{9}$$

where n is the number of iterations.

Consistent Regularization

Like many other inverse problems, the solution of Eq. (8) is often ill-conditioned. Regularization techniques are needed to provide bounds to the solution. The aim of regularization of the inverse problem is to promote certain regions of parameter space in which the model realization should exist. The two most widely used regularization methods are Tikhonov regularization [7] and truncated singular value decomposition [12].

The Tikhonov regularization expressions usually used for model updating are based on engineering assumptions on the parameter variations during iterations. The most frequently used conditions are [16] 1) $\boldsymbol{\alpha} \to 0$, i.e., that the parameter values will be small; 2) $\boldsymbol{\alpha} \to \boldsymbol{\alpha}^0$, i.e., that the total parameter changes with respect to the reference model will be small; and 3) $\Delta\boldsymbol{\alpha}^{k+1} \to 0$, i.e., that the parameter increment between iterations will be small. The incremental forms of these conditions are 1) $\Delta\boldsymbol{\alpha}^{k+1} \to -\boldsymbol{\alpha}^k$ and 2) $\Delta\boldsymbol{\alpha}^{k+1} \to \boldsymbol{\alpha}^0 - \boldsymbol{\alpha}^k$, whereas condition 3 is already in such form. Condition 1 and, to some extent, condition 2 represent physical assumptions, whereas condition 3 acts mainly as a stabilizing condition in highly nonlinear problems.

In the previously discussed side conditions, the parameter variations or the updated parameters are bounded with respect to a fixed reference vector (for example, a null or $\boldsymbol{\alpha}^0$) for all iterations. In fact, a parameter increment can be obtained from every iteration step and the structural parameter vector is updated. Some characteristics

can be found among the updated parameter vectors between iterations. For example, some elements have large values, some have small values, and some elements have fluctuating values around zero in all the iterations. These characteristics can imply that some elements are possibly damaged and some elements are undamaged. To improve the solutions in the ill-conditioned problems, these characteristics are included in the side conditions in the present study.

A new side condition is proposed that is similar to the side condition 2 mentioned previously, as follows:

$$\Delta\boldsymbol{\alpha}^{k+1} \to \boldsymbol{\alpha}^* - \boldsymbol{\alpha}^k \tag{10}$$

which implies that the total parameter change with respect to a set of reference values determined from Eq. (13) is small. Here, the reference vector $\boldsymbol{\alpha}^*$ is varying according to the results from the previous iteration steps. According to the physical definition,

$$\boldsymbol{\alpha}^k = \boldsymbol{\alpha}^0 + \sum_{i=1}^{k} \Delta\boldsymbol{\alpha}^i$$

then $\boldsymbol{\alpha}^*$ can be similarly be written as

$$\boldsymbol{\alpha}^* = \boldsymbol{\alpha}^0 + \boldsymbol{\alpha}^{k,*} \tag{11}$$

Because vector $\boldsymbol{\alpha}^0$ is the constant set of initial analytical values, it will disappear when substituting $\boldsymbol{\alpha}^*$ and $\boldsymbol{\alpha}^k$ into Eq. (10). For simplicity in the following equations, $\boldsymbol{\alpha}^k$ and $\boldsymbol{\alpha}^*$ are written as

$$\boldsymbol{\alpha}^k = \sum_{i=1}^{k} \Delta\boldsymbol{\alpha}^i, \qquad \boldsymbol{\alpha}^* = \boldsymbol{\alpha}^{k,*}$$

Eq. (10) is rewritten as

$$\Delta\boldsymbol{\alpha}^{k+1} \to \boldsymbol{\alpha}^{k,*} - \sum_{i=1}^{k} \Delta\boldsymbol{\alpha}^i \tag{12}$$

and $\boldsymbol{\alpha}^{k,*}$ is defined according to the following criteria:

$$\text{When } k = 0, \qquad \boldsymbol{\alpha}^{0,*} = 0 \tag{13a}$$

$$\begin{aligned} &\text{When } k \geq 1, \qquad \text{if } \forall\ q, (q = 1, 2, \ldots, k-1), \\ &\left(\sum_{i=1}^{q} \Delta\boldsymbol{\alpha}^i\right)_j < 0, \qquad \left|\left(\sum_{i=1}^{k} \Delta\boldsymbol{\alpha}^i\right)_j\right| \geq \text{const}, \\ &(\boldsymbol{\alpha}^{k,*})_j = \left(\sum_{i=1}^{k} \Delta\boldsymbol{\alpha}^i\right)_j, \qquad \text{otherwise } (\boldsymbol{\alpha}^{k,*})_j = 0, \\ &(j = 1, 2, \ldots, m) \end{aligned} \tag{13b}$$

The subscript j denotes the jth element of the vector, and const is a specified constant value. The physical explanation of the side condition is that the elements are categorized as two kinds of undamaged and possibly damaged elements according to the results from the previous iteration steps. Because damage in a structure is defined in terms of a stiffness-reduction factor in this study, observation with the Tikhonov regularization shows that the updated fractional stiffness change $(\boldsymbol{\alpha}^k)_j$ exhibits a definite negative value in possibly damaged elements. On the other hand, the $(\boldsymbol{\alpha}^k)_j$ of the jth undamaged element will fluctuate around zero or with small amplitudes. This characteristic of results from previous iterations is considered in the determination of $(\boldsymbol{\alpha}^{k,*})_j$ in Eq. (13). The possibly damaged elements are still updated with small incremental steps between iterations, corresponding to the type 3 side condition, and the overall parameter values for the assumed undamaged elements are kept small or the parameter change would be small with respect to zeros, which is the type 3 side condition for regularization, as discussed previously.

The conditions may be unified into the cost functions that contain the residual function and a penalty function with the updated parameter vector as

$$\begin{aligned} J(\Delta\boldsymbol{\alpha}^{k+1}, \lambda) &= \|\mathbf{S}_k \cdot \Delta\boldsymbol{\alpha}^{k+1} - (\Delta\ddot{\mathbf{h}}_l^{\text{DWT}})_k\|_2^2 \\ &\quad + \lambda^2 \|\Delta\boldsymbol{\alpha}^{k+1} - (\boldsymbol{\alpha}^{k,*} - \boldsymbol{\alpha}^k)\|_2^2 \end{aligned} \tag{14}$$

where $\boldsymbol{\alpha}^{k,*}$ is a quantity determined from results from previous k iterations shown in Eq. (13), and $\lambda \geq 0$ is the regularization parameter. The parameter λ controls the extent to which regularization is applied to the problem.

The regularization solution from minimizing the function in Eq. (14) can be written in the following form as

$$\Delta\boldsymbol{\alpha}^{k+1} = (\mathbf{S}_k^T\mathbf{S}_k + \lambda^2\mathbf{I})^{-1}(\mathbf{S}_k^T(\Delta\ddot{\mathbf{h}}_l^{\text{DWT}})_k - \lambda^2(\boldsymbol{\alpha}^k - \boldsymbol{\alpha}^{k,*})) \tag{15}$$

where the superscripts -1 and T denote the inversion and the transpose of the matrix, and $\mathbf{I}$ is the identity matrix.

Applying singular value decomposition to the sensitivity matrix $\mathbf{S}_k$, we have

$$\mathbf{S}_k = \mathbf{U}\boldsymbol{\Sigma}\mathbf{V}^T \tag{16}$$

where $\mathbf{U} \in \mathbf{R}^{\text{nt}\times\text{nt}}$ and $\mathbf{V} \in \mathbf{R}^{m\times m}$ are orthogonal matrices satisfying $\mathbf{U}^T\mathbf{U} = \mathbf{I}_{\text{nt}}$ and $\mathbf{V}^T\mathbf{V} = \mathbf{I}_m$, and $\boldsymbol{\Sigma} = \text{diag}(\sigma_1, \sigma_2, \ldots, \sigma_m)$, where the singular values σ_i $(i = 1, 2, \ldots, m)$ are arranged in a decreasing order, such that $\sigma_1 \geq \sigma_2 \geq \cdots \geq \sigma_m \geq 0$.

Then the regularization solution in Eq. (15) can be written as

$$\Delta\boldsymbol{\alpha}^{k+1} = \sum_{i=1}^{m} f_i \frac{\mathbf{U}_i^T(\Delta\ddot{\mathbf{h}}_l^{\text{DWT}})_k}{\sigma_i}\mathbf{V}_i - \sum_{i=1}^{m}(1 - f_i)\mathbf{V}_i^T(\boldsymbol{\alpha}^k - \boldsymbol{\alpha}^{k,*})\mathbf{V}_i \tag{17}$$

where $f_i = \sigma_i^2/(\sigma_i^2 + \lambda^2)$ for $i = 1, 2, \ldots, m$ are referred to as filter factors.

The solution norm

$$\|\Delta\boldsymbol{\alpha}^{k+1} - (\boldsymbol{\alpha}^{k,*} - \boldsymbol{\alpha}^k)\|_2^2$$

and the residual norm

$$\|\mathbf{S}_k \cdot \Delta\boldsymbol{\alpha}^{k+1} - (\Delta\ddot{\mathbf{h}}_l^{\text{DWT}})_k\|_2^2$$

can be expressed as

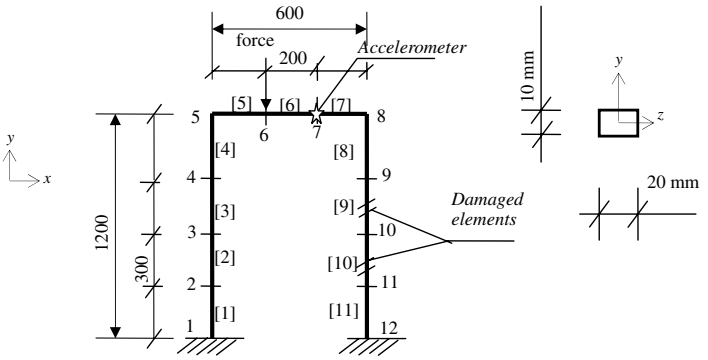

Fig. 1 One-story plane frame structure; brackets denote the element number.

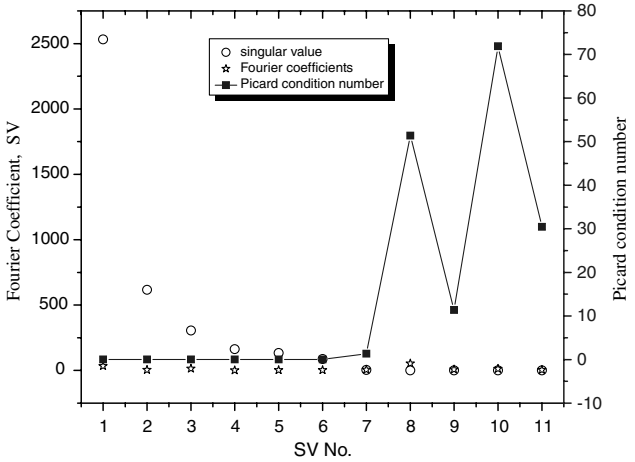

Fig. 2 Discrete SV, Fourier coefficient, and Picard condition number of the plane frame structure.

$$\eta^2 = \|\Delta\boldsymbol{\alpha}^{k+1} - (\boldsymbol{\alpha}^{k,*} - \boldsymbol{\alpha}^k)\|_2^2 = \sum_{i=1}^{m}\left(\frac{\sigma_i^2}{\sigma_i^2+\lambda^2}\left(\frac{\mathbf{U}_i^T(\Delta\ddot{\mathbf{h}}_l^{\mathrm{DWT}})_k}{\sigma_i} + \mathbf{V}_i^T(\boldsymbol{\alpha}^k - \boldsymbol{\alpha}^{k,*})\right)\right)^2 \quad (18)$$

$$\rho^2 = \|\mathbf{S}_k\cdot\Delta\boldsymbol{\alpha}^{k+1} - (\Delta\ddot{\mathbf{h}}_l^{\mathrm{DWT}})_k\|_2^2 = \sum_{i=1}^{m}\left(\frac{\lambda^2}{\sigma_i^2+\lambda^2}(\mathbf{U}_i^T(\Delta\ddot{\mathbf{h}}_l^{\mathrm{DWT}})_k + \mathbf{V}_i^T(\boldsymbol{\alpha}^k - \boldsymbol{\alpha}^{k,*})\sigma_i\right)^2 + (\Delta\ddot{\mathbf{h}}_l^{\mathrm{DWT}})_k^T\cdot(\mathbf{I}-\mathbf{U}\mathbf{U}^T)\cdot(\Delta\ddot{\mathbf{h}}_l^{\mathrm{DWT}})_k \quad (19)$$

These two quantities represent the smoothness and goodness of fit of the solution, and they should be balanced by choosing an appropriate regularization parameter.

The determination of the regularization parameter λ can be determined by different techniques such as the L-curve method [8] and cross-validation. The L-curve method finds the appropriate regularization parameter by maximizing the curvature function:

$$\frac{\mathrm{d}\theta}{\mathrm{d}s} = \frac{\rho'\eta'' - \eta'\rho''}{((\rho')^2 + (\eta')^2)^{1.5}} \quad (20)$$

where $\eta' = \mathrm{d}\eta/\mathrm{d}\lambda$, $\rho' = \mathrm{d}\rho/\mathrm{d}\lambda$, $\eta'' = \mathrm{d}^2\eta/\mathrm{d}\lambda^2$, and $\rho'' = \mathrm{d}^2\rho/\mathrm{d}\lambda^2$, with a limitation imposed on the range of λ (i.e., $\sigma_1 \geq \lambda \geq \sigma_n$). Finally, the optimal regularized solution $\Delta\boldsymbol{\alpha}^{k+1}$ is determined from Eq. (15) or Eq. (17).

If the system carries no noise and no model error, the regularization parameter λ determined from Eq. (20) is correct. When there is noise and model error, the regularization parameter λ so obtained will lead to a regularized solution that is beyond the physical range. For example, the stiffness-reduction factor has a limited range of $-1.0 \leq \Delta\alpha \leq 0.0$. The regularized solutions determined by the previous λ are not in the range of $[-1.0, 0.0]$. Some sorts of constraints are needed in the process of finding the appropriate regularization parameter λ.

Such a constraint is defined as

$$\mathbf{V}_L \leq \boldsymbol{\alpha}^k + \Delta\boldsymbol{\alpha}^{k+1}(\lambda) \leq \mathbf{V}_U \quad (21)$$

where $\boldsymbol{\alpha}^k$ is given in Eq. (12), $\Delta\boldsymbol{\alpha}^{k+1}(\lambda)$ is given in Eq. (15) or Eq. (17), and $\mathbf{V}_L \in \mathbf{R}^{m\times 1}$ and $\mathbf{V}_U \in \mathbf{R}^{m\times 1}$ are the given lower and upper limit vectors, respectively. Because the local damage is often represented by a percentage change in the system parameters and

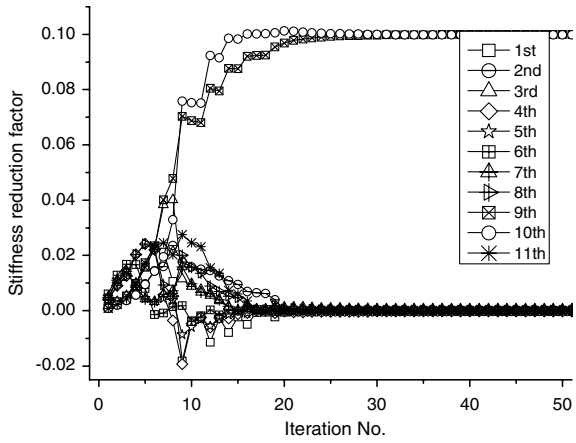

a) From consistent regularization

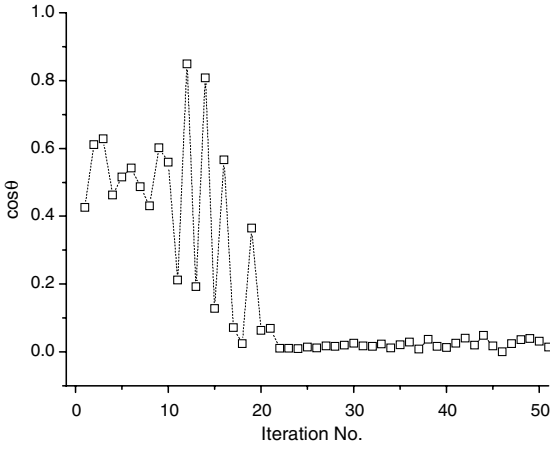

b) cosθ for consistent reguration

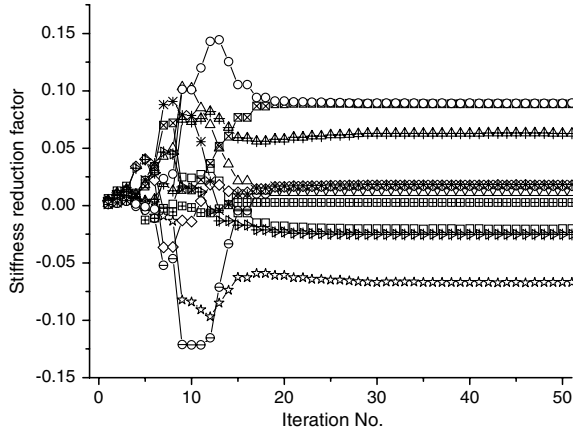

c) From Tikhonov regularization

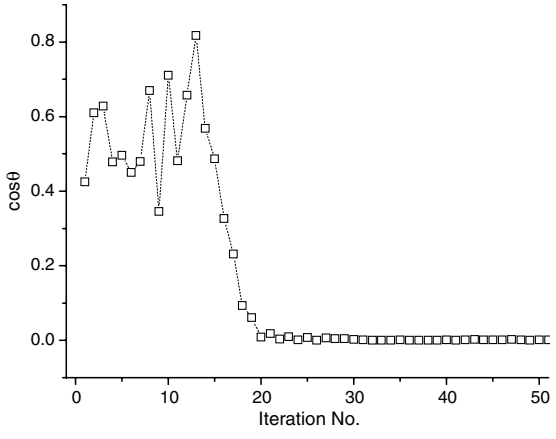

d) cosθ for Tikhonov regulation

Fig. 3 Evolution of identified results and cos θ from the consistent, and Tikhonov regularization methods when there is 1% noise.

each component of the damage vector is always less than unity, we can set $\mathbf{V}_L$ and $\mathbf{V}_U$ as

$$\mathbf{V}_L = [-1 \quad -1 \quad \cdots \quad -1]^T, \qquad \mathbf{V}_U = [1 \quad 1 \quad \cdots \quad 1]^T \quad (22)$$

If a narrower range is needed, $\mathbf{V}_U$ can be set smaller, closer to zero. The constraint in Eq. (21) can also be expressed as the range of the regularization parameter. From Eq. (17), the filter factors f_i influence the identified results together with λ. When λ increases, f_i will decrease and $\Delta\boldsymbol{\alpha}^{k+1}(\lambda)$ will decrease, where $\boldsymbol{\alpha}^k + \Delta\boldsymbol{\alpha}^{k+1}(\lambda)$ will have a small change and it would be more likely to be within the physical range of changes. Therefore, Eq. (21) corresponds to

$$\sigma_1 \geq \lambda \geq \text{const2} \quad (23a)$$

instead of

$$\sigma_1 \geq \lambda \geq \sigma_n \quad (23b)$$

where const2 is determined from Eq. (17) by a numerical method to be discussed later. When the allowable range is found, λ is determined by finding the local maximal curvature expressed by Eq. (20).

In general, there is one turning point in the L-curve corresponding to the point of maximal peak, and λ is easily obtained from the point with the maximal curvature. The L-curve may have several points with a local peak, and some of them may be caused by measurement noise or other errors and would lead to erroneous results if selected. These peak values may be larger than the local peak value corresponding to the correct optimal regularization parameter.

There may be many other techniques that can be used to select the correct local peak points on the L-curve. When there are several local peaks in the curvature curve, the point with the regularization parameter closest to the optimal regularization parameter for the immediately past iteration is chosen as the optimal point for the present iteration. This is based on the assumption that the incremental change of the parameter would be small. Finally, the regularized solution $\Delta\boldsymbol{\alpha}^{k+1}$ is determined from Eq. (17).

Convergence Criterion

A stopping criterion based on the gradient of the residual and penalty functions is adopted [12,17]. Two augmented matrices are defined as

$$\mathbf{A}_k = \begin{bmatrix} \mathbf{S}_k \\ \lambda_k \mathbf{I} \end{bmatrix}, \qquad \mathbf{R}_k = \begin{bmatrix} (\Delta \ddot{\mathbf{h}}_l^{\mathrm{DWT}})_k \\ -\lambda_k(\Delta\boldsymbol{\alpha}^{k+1} - (\boldsymbol{\alpha}^{k,*} - \boldsymbol{\alpha}^k)) \end{bmatrix} \quad (24)$$

The angle between the subspace spanned by $\mathbf{A}$ and $\mathbf{R}$ is given by Dennis and Schnabel [17]:

$$\cos\theta = \frac{\mathbf{R}_k^T \cdot (\mathbf{A}_k \cdot \Delta\boldsymbol{\alpha}^{k+1})}{\|\mathbf{R}_k\|_2 \cdot \|\mathbf{A}_k \cdot \Delta\boldsymbol{\alpha}^{k+1}\|_2} \quad (25)$$

The iteration is said to converge if $\cos\theta$ is less than a tolerance value. The convergence for the present study is considered to be achieved when $\cos\theta$ approaches a stable value with iterations.

Simulation Studies

A one-story plane frame structure shown in Fig. 1 is used for the simulation study. The finite element model of the structure consists of four and three equal beam-column elements in each vertical and horizontal member, respectively. The columns of the frame are 1.2 m high and the cross beam is 0.6 m long, and each member has a 10 mm

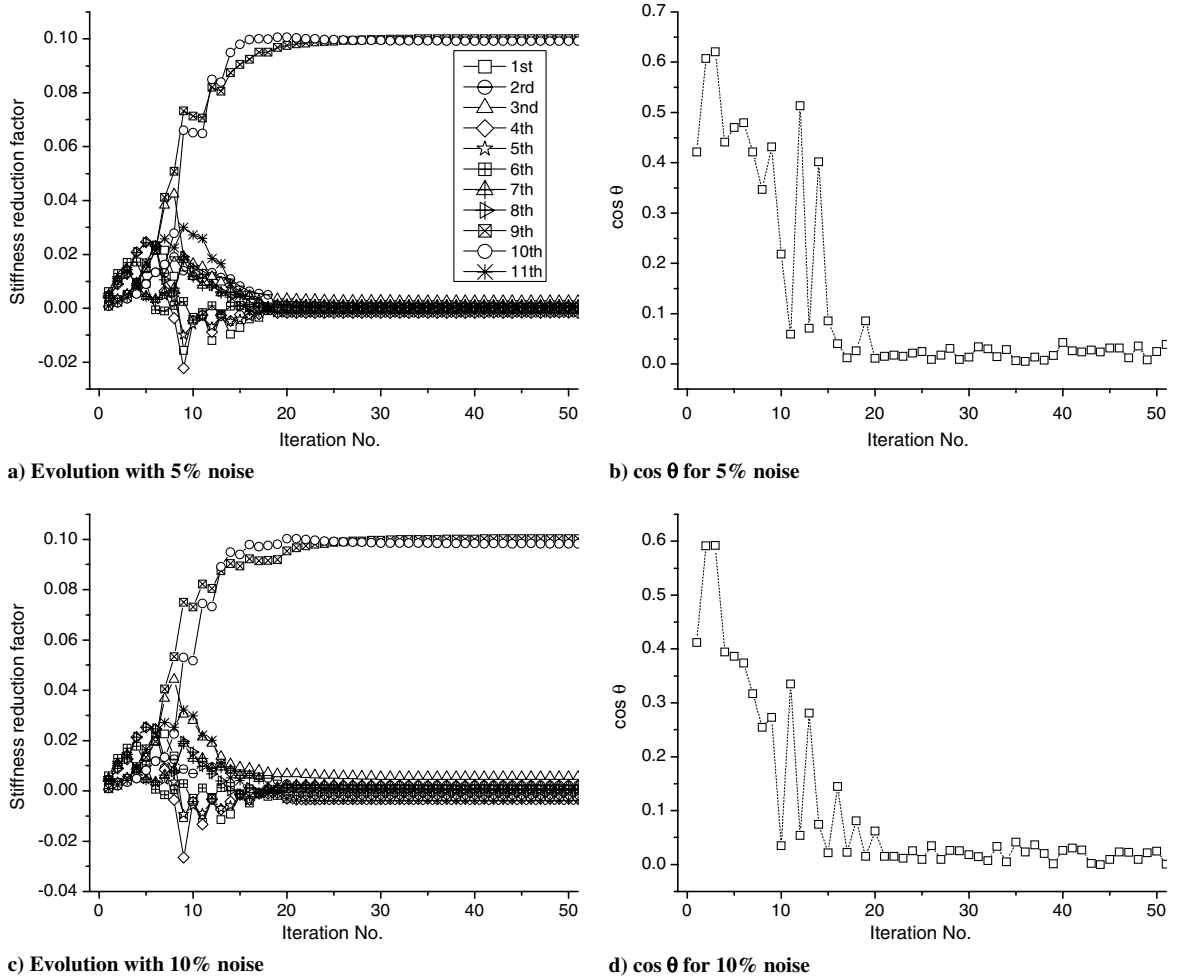

a) Evolution with 5% noise

b) cos θ for 5% noise

c) Evolution with 10% noise

d) cos θ for 10% noise

Fig. 4 Evolution of identified results and cos θ from consistent regularization with 5 and 10% noise.

depth and 20 mm breadth uniform rectangular cross section. The modulus of elasticity and the mass density of materials are, respectively, 69×10^9 N/m^2 and 2700 kg/m^3. The horizontal, vertical, and rotational restraints at the supports are represented by large stiffnesses of 1.5×10^{10} kN/m, 1.5×10^9 kN/m, and 1.5×10^7 kN-m/rad, respectively. Rayleigh damping is adopted for the system with the two modal damping ratios $\xi_1 = \xi_2 = 0.01$ for the first two modal frequencies. The first 12 natural frequencies of the structure are 13.09, 57.29, 76.68, 152.38, 196.43, 227.28, 374.59, 382.42, 580.05, 699.10, 764.79, and 977.69 Hz.

The structure is subject to a sinusoidal excitation $F(t) = 10 \sin(12\pi t)N$ applied vertically at node 6, as shown in Fig. 1. The vertical acceleration at node 7 is recorded for the study. The sampling frequency is 2000 Hz, which is high enough to avoid computational error from using the Newmark method, and 0.25 s of measured data are used. There are 500 data points of acceleration response corresponding to 500 DWT coefficients of the IRF with the Daubechies wavelet.

A damage scenario with 10% stiffness reduction in both the ninth and tenth elements is studied, as shown in Fig. 1. Different levels of random noise and model errors are included, and the proposed regularization method and the Tikhonov regularization with side condition 3 are used to compute the inverse problems. The results from both methods are compared to illustrate the application of the proposed method to ill-posed problems. Because the acceleration responses from the damaged state are obtained by computation instead of measurement in this paper, the measurement errors are simulated with white noise added to the calculated accelerations as

$$\ddot{\mathbf{x}}_{\text{measured}} = \ddot{\mathbf{x}}_{\text{calculated}} + Ep^* \mathbf{N}^*_{\text{oise}} \text{var}(\ddot{\mathbf{x}}_{\text{calculated}}) \qquad (26)$$

where $\ddot{\mathbf{x}}_{\text{measured}}$ is the vector of polluted acceleration, Ep is the noise level, $\mathbf{N}_{\text{oise}}$ is a standard normal distribution vector with zero mean and unit standard deviation, var$(\cdot)$ is the variance of the time history, and $\ddot{\mathbf{x}}_{\text{calculated}}$ is the vector of calculated acceleration responses from the damaged state of the structure.

The frame structure is statically indeterminate. Figure 2 plots the discrete singular values (SVs) σ_i, Fourier coefficient $|\mathbf{U}(:, i)^T \cdot \boldsymbol{\Delta} \ddot{\mathbf{h}}_l^{\text{DWT}}|$, and Picard condition number, defined as the ratio of the Fourier coefficient to the corresponding SV at the first iteration step for model updating. It is seen that the Fourier coefficients for the lower-order SVs remain relatively constant around the order of 10, whereas they decay gradually with increasing order with their singular values. This leads to very large values for the last four orders of the discrete Picard condition. The discrete Picard condition is not satisfied, and regularization methods must be applied to obtain a regularized and stable solution.

Case 1: Low Noise Level

One-percent random white noise is added to the structural acceleration responses obtained from the damaged structure from Eq. (26) to simulate the low noise effect in the inverse problem. The evolution of reduction factors of all elements with iterations is shown in Fig. 3a for the consistent regularization and in Fig. 3c for the traditional Tikhonov regularization. It can be seen that the reduction factors of the two damaged elements converge to the true value after about 20 iterations and remain constant with increasing iterations for both regularization methods. The evolution of reduction factors for other intact elements converges to 0 after about 20 iterations in the consistent regularization method, but not in the Tikhonov regularization, in which some results converge to nonzero values (for example, the seventh element converges to 0.06 and the fifth

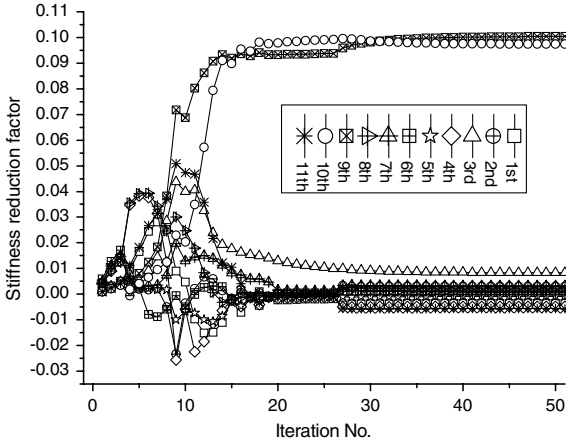

a) Evolution with 15% noise

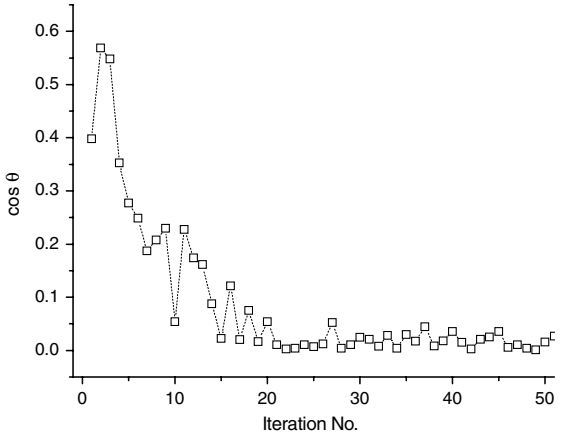

b) cos θ for 15% noise

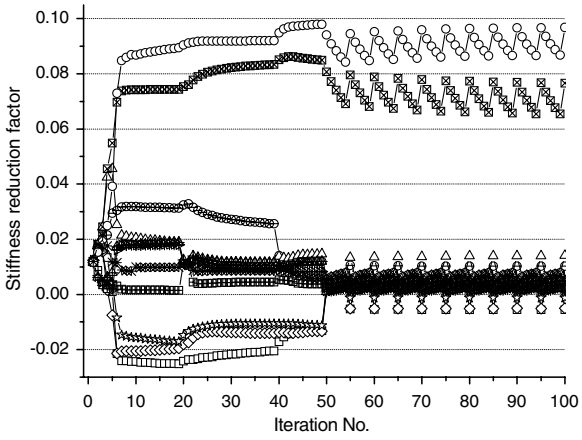

c) Evolution with 15% noise + model errors

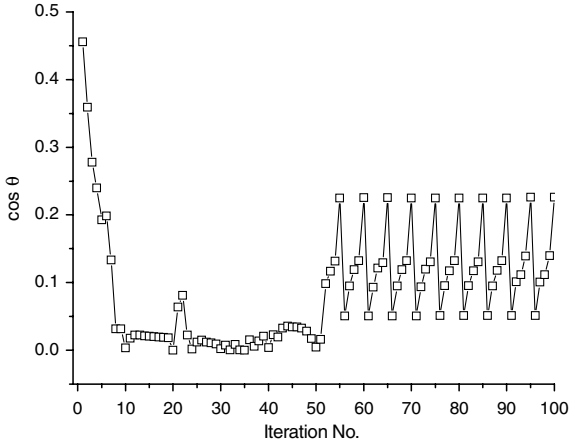

d) cos θ with 15% noise + model errors

Fig. 5 Evolution of identified results and cos θ from consistent regularization with 15% noise and 15% noise plus model error.

element converges to −0.06). It is obvious that the consistent method is superior to the traditional Tikhonov regularization in this exercise. The evolution of the stopping-criteria value ($\cos\theta$) computed by Eq. (25) with iterations is shown in Figs. 3b and 3d for the two methods. The value of $\cos\theta$ is noted to fluctuate at the beginning and to finally converge to a value close to zero in both methods. When $\cos\theta$ arrives at a steady value, it means that the iteration is converging. The damaged vectors can then be obtained easily from results obtained from any iteration after the critical iteration.

Case 2: Median Noise Level

Five and 10% noise levels are added separately to the computed acceleration responses of the damaged structure to simulate more severe noise effect. The evolution of stiffness-reduction factor for all elements and the stopping criteria for the consistent regularization method are shown in Fig. 4. The evolution of results for the consistent regularization method is similar to the last case with 1% noise and is a little bit poorer. The application of the consistent regularization method is shown to be able to reduce the noise effect greatly.

Case 3: High Noise Level and Model Errors

The noise level is further increased to 15%, and the results from the consistent regularization method are shown in Figs. 5a and 5b. Compared with those from 1, 5, and 10% noise levels, the results become a little bit poorer but are still very good. Model error is then introduced with 1% underestimation in the stiffnesses of all elements of the structure. The 15% noise level remains in the responses, and the identified results from the consistent method are shown in Figs. 5c and 5d. It can be seen that the results arrive at the steady values after about 50 iterations. With further iterations beyond the 50th iteration, the stiffness-reduction factor and the stopping-criteria value $\cos\theta$ fluctuate greatly around the stable values at the 50th iteration. The results after the 50th iteration are not very good, but this fluctuating behavior provides an indication of an acceptable set of converged results before their occurrences, i.e., at the 50th iteration.

Results from the traditional Tikhonov regularization method for cases 2 and 3 are getting worse compared with case 1, with many false positives in other elements and with the identified damage extent increasing with increasing noise level. However, the damaged elements can still be identified with correct damage extent in the presence of the different noise levels, and they are not shown.

Optimal Regularization Parameter

The optimal regularization parameters for every iteration step in the previous cases with 1, 5, 10, and 15% noise and 15% noise plus model errors using the consistent method and traditional Tikhonov regularization are shown in Fig. 6. The pattern of variation of the regularization parameter for the four noise levels from the consistent method shown in Fig. 6a are similar, with only the case with 15% noise showing some differences. The case with 1% noise from traditional Tikhonov regularization shown in Fig. 6c has similar pattern to Fig. 6a in the first 10 iterations. However, the 11th to 15th regularization parameters in Fig. 6c are smaller compared with those in Fig. 6a, which may mean that the large perturbations in the parameter increment vectors due to the ill-conditioning are less restrained, leading to a set of poorer identified results. The case with 15% noise plus model errors is shown in Fig. 6b. The pattern is completely different from the case with only 15% noise. This again indicates that model error has a large effect on the identified results.

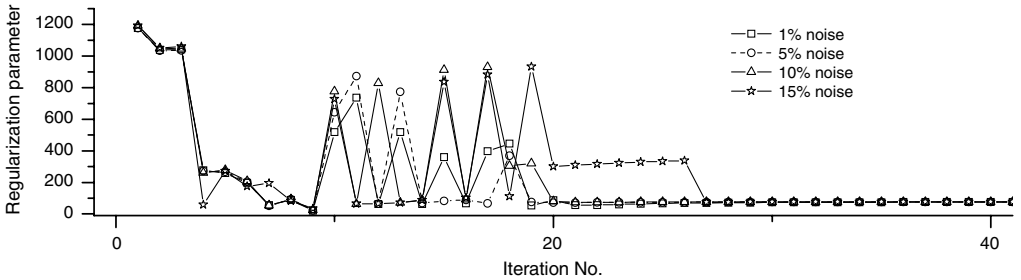

a) Regularization parameters using consistent regularization with different noise levels

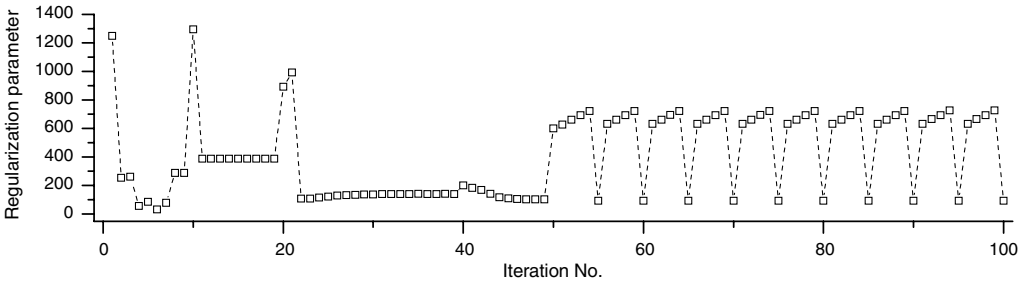

b) Regularization parameters using consistent regularization with 15% noise + model errors

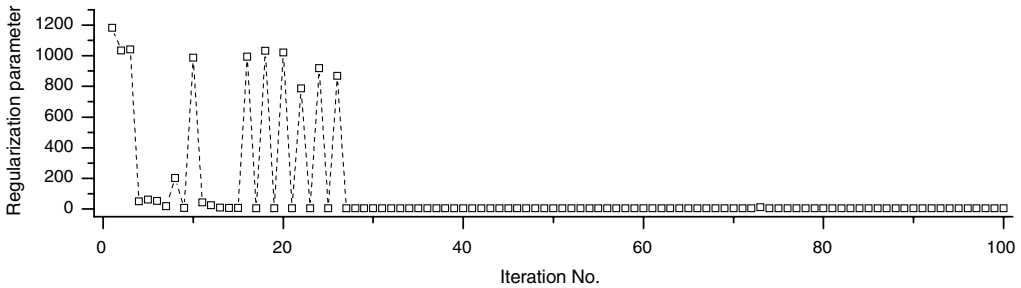

c) Regularization parameters using tikhonov method with 1% noise

Fig. 6 Evolution of optimal regularization parameters from consistent method and Tikhonov method.

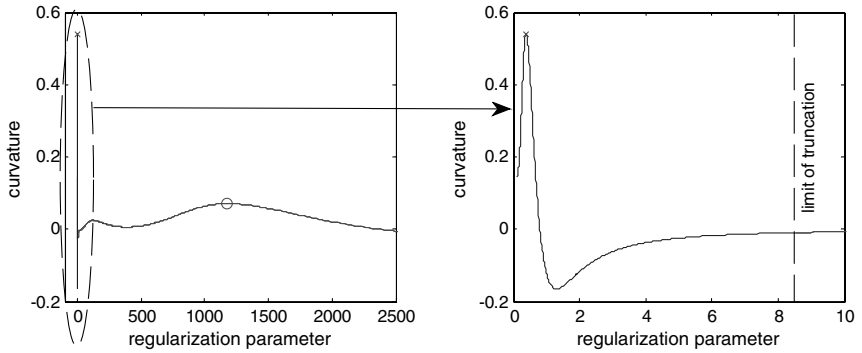

a) The whole curvature curve **b) Part of the curvature curve that is rejected**

Fig. 7 Curvature after the first iteration with 1% noise level.

Determination of the Regularization Parameter Range

To illustrate the application of Eqs. (21–23) in determining the regularization parameter range and the optimal parameter, the curvature of the L-curve, after the first iteration for the case with 1% noise using the consistent method and Tikhonov regularization method is shown in Fig. 7. Figure 7a shows the complete curvature curve and Fig. 7b gives part of the curvature curve that is rejected according to the requirements in Eq. (21), in which the cutoff point is computed from Eqs. (17) and (21) by the following method.

The range $[\sigma_n, \sigma_1]$ is divided into 800 divisions, and there are 801 discrete values that may be taken up by λ in Eq. (17). The computation starts with the smallest value to check whether the resulting $\boldsymbol{\Delta\alpha}^{k+1}$ would be within the specified range of $[-1.0, 0.0]$. The smallest value that satisfies the requirement mentioned previously is considered the limiting constant, const2 in Eq. (23), and the optimal regularization parameter is selected within the range of $\sigma_1 \geq \lambda \geq$ const2.

The hollow circle denotes the optimal regularization parameter. The symbol X denotes the maximal curvature point. When optimal regularization parameter is searched on the whole L-curve in the Tikhonov regularization, the point marked by X is selected, and the corresponding regularization parameter 0.3883 will be the optimal regularization parameter. This parameter would lead to results that are not in the physical range, which means that some stiffness-reduction factor is greater than 1.0 or less than -1.0 and the iteration cannot continue. This is usually termed in computation as a *diverged solution*. When the optimal point is searched in the truncated curvature curve, the point marked by o is selected, and the obtained results from the consistent regularization method and traditional Tikhonov regularization adopting this selection process shown in Figs. 3a and 3c are satisfactory. This approach of consistently selecting the optimal regularization parameter is also applied to other cases using the consistent regularization method.

Consistent Selection of the Optimal Regularization Parameter

After the correct range of the regularization parameter λ is determined as discussed previously, the optimal regularization parameter can be chosen correctly. The application of the consistent selection of the optimal regularization parameter is illustrated by plotting the L-curve and the corresponding curvature curve for the first 24 iterations for the case with 1% noise level shown in Figs. 8–10. The identified results converge to the steady values after 24 iteration steps.

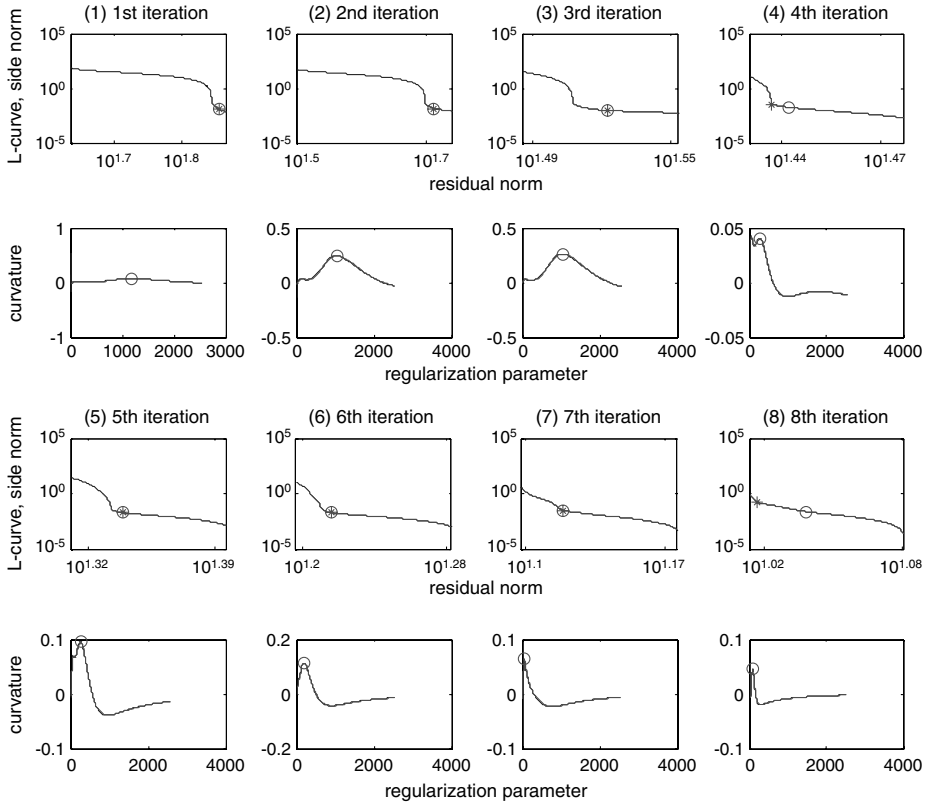

Fig. 8 L-curve and curvature in the first–eighth iteration steps for the case with 1% noise.

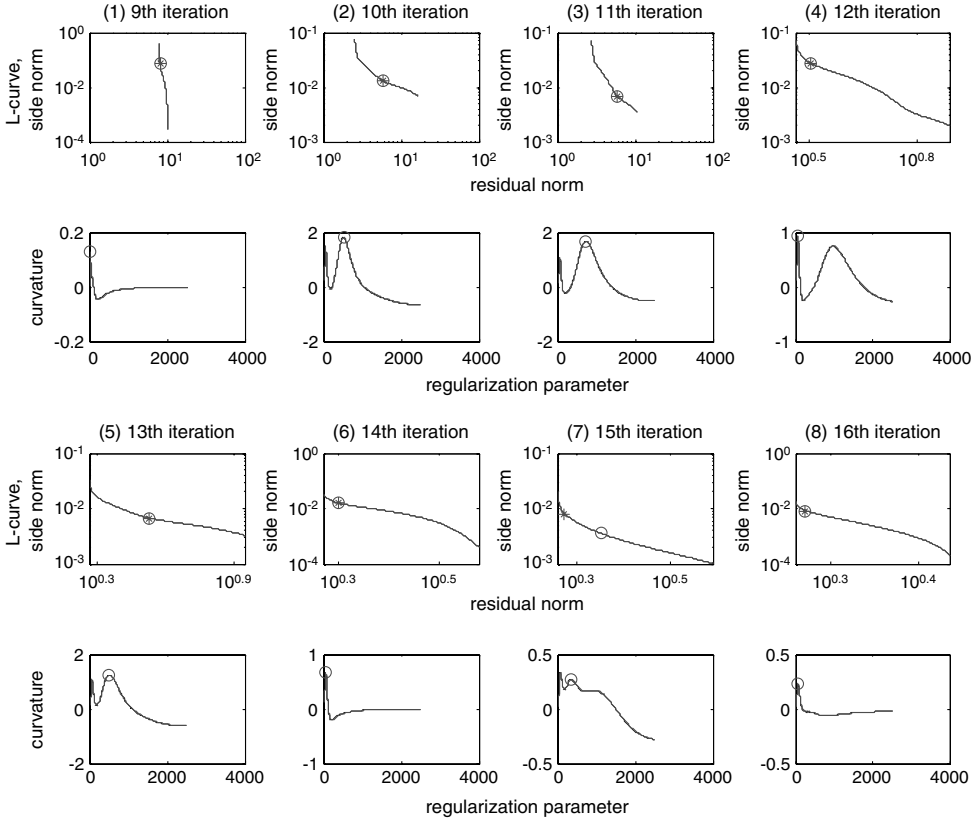

Fig. 9 ***L*-curve and curvature in the 9th–16th iteration steps for the case with 1% noise.**

The solid line denotes the whole curve and the dashed line denotes the truncated curve according to Eq. (21), and they are overlapping in the figures. The point marked by o denotes the optimal turning point from using the consistent-selection technique together with the new side condition in Eq. (13). The point marked by $*$ is determined from using the new side condition in Eq. (13) only.

It can be seen that the points marked by o and $*$ are overlapped in the first to third iterations, whereas the two points are separated in the fourth iteration. The identified damage vectors from each iteration step by the two methods are shown in Tables 1 and 2. It can be seen that the damage vectors from the first three iterations are identical between the two methods, whereas obvious difference happens in the

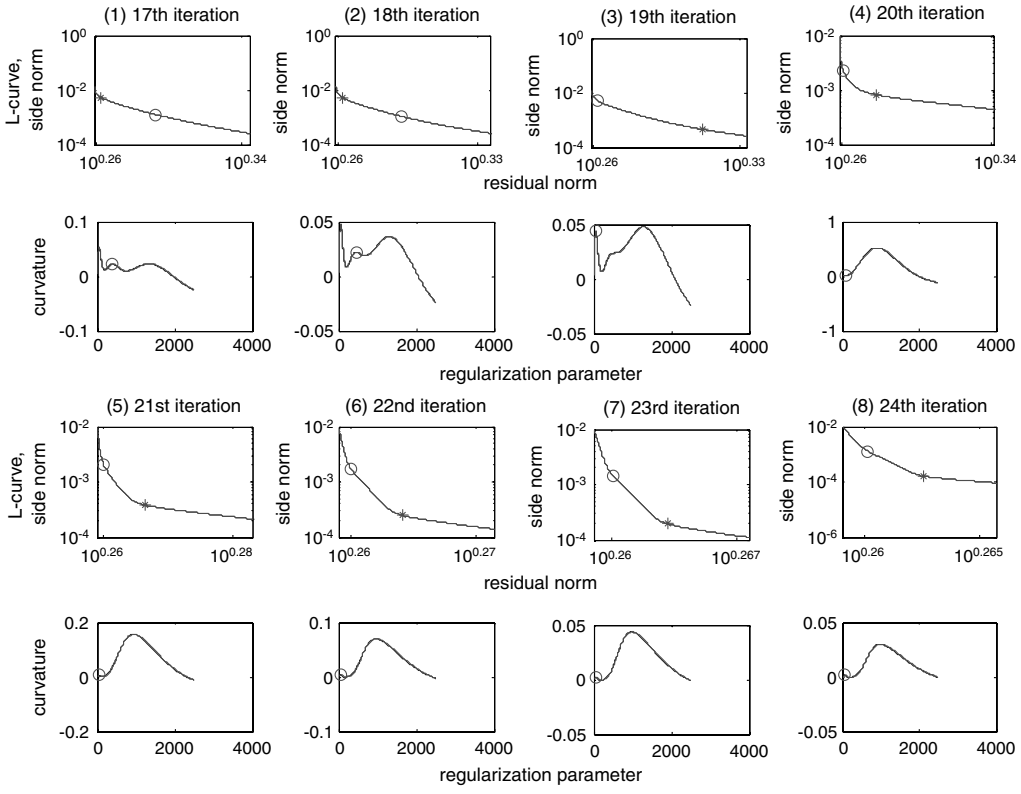

Fig. 10 ***L*-curve and curvature in the 17th–24th iteration steps for the case with 1% noise.**

Table 1 Damage vectors from first 24 iterations using the new side condition and the consistent regularization selection technique: iteration steps 1–12

Element number	Iteration steps 1	2	3	4	5	6	7	8	9	10	11	12
Consistent method using both techniques												
1	9.0E − 04	0.0023	0.0042	0.0098	0.0173	0.0234	0.0212	0.0106	−0.0182	−0.0037	−0.0018	−0.0115
2	9.0E − 04	0.0021	0.0036	0.0057	0.0098	0.0144	0.016	0.0236	0.0177	0.0158	0.0149	0.0145
3	0.0015	0.0033	0.0053	0.0099	0.0157	0.0228	0.0382	0.0401	0.0114	0.0088	0.0076	0.0055
4	0.0041	0.009	0.0126	0.0204	0.0241	0.022	0.0056	−0.0036	−0.0193	−0.0046	−0.0024	−0.0061
5	0.0049	0.011	0.0142	0.0084	0.0044	0.0033	0.0044	0.0036	−0.0087	−0.0061	−0.0032	−0.0056
6	0.0061	0.0128	0.0168	0.0167	0.0081	−0.0014	−8.0E − 04	0.0014	0.0019	−0.0039	−0.0022	3.0E − 04
7	0.0048	0.011	0.0142	0.0084	0.0043	0.0033	0.0059	0.0072	0.0158	0.0098	0.0066	0.0062
8	0.0041	0.009	0.0126	0.0204	0.0241	0.0221	0.0093	0.0052	0.02	0.0157	0.0135	0.0089
9	0.0015	0.0033	0.0053	0.0099	0.0156	0.0228	0.0401	0.0478	0.0703	0.0688	0.0681	0.0805
10	8.0E − 04	0.002	0.0036	0.0056	0.0095	0.0142	0.0195	0.0329	0.0758	0.0753	0.0751	0.0923
11	9.0E − 04	0.0023	0.0042	0.0097	0.0172	0.0234	0.0245	0.0202	0.0275	0.0246	0.0231	0.0155
Consistent method using only the new side condition												
1	9.0E − 04	0.0024	0.0042	0.0106	0.0226	0.0227	0.0306	0.0303	−0.0256	−0.0082	−0.0033	−0.0019
2	9.0E − 04	0.0021	0.0036	2.0E − 04	−0.0031	0.0	−0.0049	−2.0E − 04	−0.0494	−0.0051	−0.0016	−1.0E − 03
3	0.0015	0.0033	0.0053	0.0099	0.0173	0.0171	0.0321	0.0319	0.0201	0.0134	0.0117	0.0106
4	0.0041	0.009	0.0126	0.0332	0.0398	0.0383	0.0189	0.0176	−0.046	−0.0122	−0.007	−0.0039
5	0.0049	0.011	0.0143	0.006	0.0037	0.0012	0.0035	0.0018	−0.0278	−0.0156	−0.0093	−0.0049
6	0.006	0.0128	0.0168	0.0067	−0.0134	−0.0025	−0.0084	−0.0017	−7.0E − 04	−0.0114	−0.0075	−0.0043
7	0.0048	0.0109	0.0142	0.0054	0.004	0.0015	0.0054	0.0037	0.0374	0.021	0.011	0.0059
8	0.0041	0.009	0.0127	0.0347	0.042	0.0405	0.0258	0.0245	0.0509	0.0396	0.0325	0.0287
9	0.0015	0.0034	0.0053	0.0091	0.0175	0.0174	0.0351	0.0349	0.0907	0.0869	0.0845	0.0831
10	8.0E − 04	0.002	0.0036	2.0E − 04	−0.0031	0.0	−9.0E − 04	−1.0E − 04	0.0422	−7.0E − 04	−0.0014	−9.0E − 04
11	9.0E − 04	0.0023	0.0042	0.01	0.0222	0.0223	0.0349	0.0346	0.0954	0.0891	0.0853	0.0832

Table 2 Damage vectors from first 24 iterations using the new side condition and the consistent regularization selection technique: iteration steps 13–24

Element number	Iteration steps 13	14	15	16	17	18	19	20	21	22	23	24
Consistent method using both techniques												
1	−0.0028	−0.0079	−0.0023	−0.0049	−7.0E − 04	−5.0E − 04	−0.0022	−5.0E − 04	−4.0E − 04	−4.0E − 04	−4.0E − 04	−3.0E − 04
2	0.0126	0.0109	0.0095	0.0069	0.0065	0.0062	0.004	4.0E − 04	1.0E − 04	1.0E − 04	1.0E − 04	2.0E − 04
3	0.0035	0.0012	−0.0011	8.0E − 04	−2.0E − 04	−2.0E − 04	7.0E − 04	0.0012	0.0013	0.0012	1.0E − 03	9.0E − 04
4	−0.0025	−0.0028	−0.0013	−8.0E − 04	0.0	0.0	−9.0E − 04	−3.0E − 04	−5.0E − 04	−5.0E − 04	−4.0E − 04	−4.0E − 04
5	−0.0025	−0.0016	−2.0E − 04	−1.0E − 03	4.0E − 04	3.0E − 04	−8.0E − 04	−2.0E − 04	−4.0E − 04	−3.0E − 04	−2.0E − 04	−2.0E − 04
6	−0.0015	2.0E − 04	−1.0E − 04	5.0E − 04	4.0E − 04	4.0E − 04	1.0E − 04	1.0E − 04	1.0E − 04	1.0E − 04	1.0E − 04	1.0E − 04
7	0.0039	0.0015	1.0E − 04	0.0012	5.0E − 04	5.0E − 04	1.0E − 03	4.0E − 04	5.0E − 04	4.0E − 04	4.0E − 04	3.0E − 04
8	0.0069	0.0052	0.0046	0.0016	3.0E − 04	3.0E − 04	0.0018	6.0E − 04	7.0E − 04	6.0E − 04	4.0E − 04	3.0E − 04
9	0.0795	0.0877	0.0875	0.0921	0.0923	0.0925	0.0955	0.0969	0.0978	0.0983	0.0987	0.099
10	0.0915	0.0986	0.0983	0.1001	0.1001	0.1002	0.1006	0.1013	0.1011	0.1008	0.1006	0.1004
11	0.0136	0.0074	0.0061	0.0035	−2.0E − 04	−1.0E − 04	−1.0E − 04	−1.0E − 04	−4.0E − 04	−4.0E − 04	−4.0E − 04	−4.0E − 04
Consistent method using only the new side condition												
1	−0.0011	−0.0092	−0.0148	−0.0178	−0.0157	−0.0132	−0.0113	−0.0094	−0.0093	−0.0093	−0.0093	−0.0093
2	−6.0E − 04	8.0E − 04	0.0051	0.0124	0.017	0.0204	0.0207	0.0201	0.0203	0.0204	0.0204	0.0204
3	0.0099	0.0236	0.0214	0.01	−0.0049	−0.0111	−0.0123	−0.0134	−0.0137	−0.0138	−0.0139	−0.0139
4	−0.0023	−0.018	−0.015	−0.0075	0.0044	0.0079	0.0068	0.0054	0.0055	0.0055	0.0055	0.0055
5	−0.0027	4.0E − 04	−9.0E − 04	−0.0029	−0.0068	−0.0054	−0.0032	−2.0E − 04	1.0E − 04	2.0E − 04	2.0E − 04	2.0E − 04
6	−0.0026	−0.0012	0.0011	0.0032	0.0033	0.0017	0.0011	7.0E − 04	7.0E − 04	7.0E − 04	7.0E − 04	7.0E − 04
7	0.0031	0.0036	0.0044	0.005	0.0073	0.0057	0.0037	6.0E − 04	3.0E − 04	3.0E − 04	2.0E − 04	2.0E − 04
8	0.0265	0.0187	0.0081	−0.0036	−0.0147	−0.0139	−0.0114	−0.0092	−0.0092	−0.0092	−0.0093	−0.0092
9	0.0824	0.0927	0.0985	0.1069	0.1186	0.1203	0.1205	0.1217	0.1222	0.1224	0.1225	0.1225
10	−5.0E − 04	0.0073	0.0237	0.0453	0.0678	0.0777	0.0787	0.0791	0.0788	0.0787	0.0786	0.0786
11	0.082	0.0778	0.0687	0.0524	0.0273	0.0113	0.0075	0.0048	0.0046	0.0046	0.0046	0.0046

fourth iteration, due to the different optimal regularization parameter found in Fig. 8. When the iteration continues, the optimal points from both methods are different in the 8th, 15th, and 17th–24th iterations. The final results, shown in Fig. 3a, from using both proposed techniques are very good, and the results using only the new side condition shown in Fig. 11 are acceptable, with one false alarm at the second element with 0.0204 stiffness reduction and with some error in the damage extent. The consistent-selection technique in addition to the new side condition is shown to be better than the new side condition only in obtaining a good and converged set of identified results. It can be concluded from this study that the consistent-selection technique can ensure a stable model updating for obtaining good updated parameter vectors, and the new side condition in Eq. (13) can increase the speed of convergence of the solution.

The final identified damage vectors using the consistent method and Tikhonov method with different levels of noise plus model errors are shown in Table 3. It can be seen that the results using the proposed two techniques are very good even if there is 15% noise plus model error. However, the results from Tikhonov method with side condition 3 and traditional L-curve method have many false alarms, especially in the cases with 5 and 10% noise levels, with the largest false alarm occurring at the seventh element.

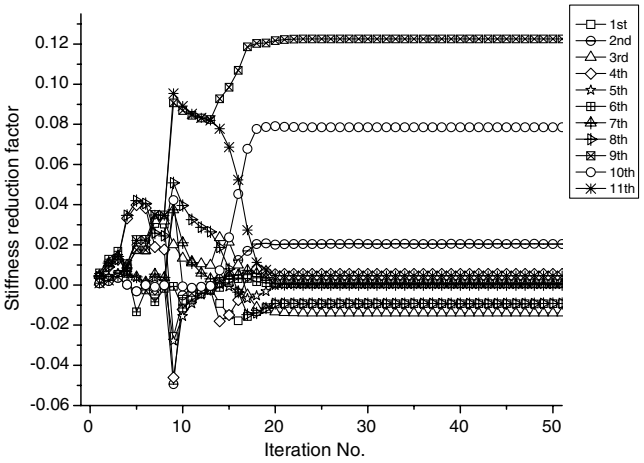

Fig. 11 Evolution of stiffness-reduction factor for all elements using only the new side condition.

Table 3 Damage vectors obtained from the consistent method and Tikhonov method

	1% noise		5% noise		10% noise		15% noise	15% noise plus model error
Element number	Consistent method	Tikhonov method	Consistent method	Tikhonov method	Consistent method	Tikhonov method	Consistent method	
1	−3.0E − 04	−0.0193	−0.0013	−0.0297	−0.0025	−0.0349	−0.0035	−0.0055
2	2.0E − 04	0.0155	0.0011	0.0309	0.0022	0.0501	0.0031	0.0102
3	6.0E − 04	0.0111	0.0028	0.0254	0.0056	0.0314	0.0084	0.014
4	−3.0E − 04	0.017	−0.0016	0.0182	−0.0033	0.0118	−0.0048	−0.005
5	−1.0E − 04	−0.0642	−3.0E − 04	−0.1345	−7.0E − 04	−0.1907	−9.0E − 04	−0.0014
6	1.0E − 04	0.0027	4.0E − 04	6.0E − 04	8.0E − 04	−0.0019	0.0012	0.0019
7	2.0E − 04	0.0604	0.0011	0.1176	0.0021	0.1577	0.0032	0.005
8	1.0E − 04	−0.0245	4.0E − 04	−0.024	6.0E − 04	−0.017	8.0E − 04	0.0048
9	0.1	0.0889	0.1001	0.0713	0.1002	0.0654	0.1004	0.0766
10	0.0998	0.0899	0.0992	0.0848	0.0983	0.0735	0.0974	0.0968
11	−3.0E − 04	0.0177	−0.0018	0.0155	−0.0037	0.0084	−0.0056	1.0E − 03

Conclusions

In this paper, a new side condition is proposed that classified the identified elements as possibly damaged and undamaged elements from results obtained from previous iterations. The possibly damaged elements are improved with small steps between iterations, and the parameters for the undamaged elements are required to approach zero. These measures can make the updating procedure converge to the real values more quickly and accurately. In addition, the range of the regularization parameter is computed in advance, and the optimal point on the curvature curve is consistently selected to ensure that the updating procedure is performed on the right path and that the parameters are improved accordingly. It can be seen from the numerical studies that the proposed method using both techniques can give very accurate results in an ill-conditioned inverse problem with high levels of noise and model errors, whereas with the conventional Tikhonov regularization method, the identified parameters in the undamaged elements fluctuate greatly around zero, and the incorrect optimal point on the L-curve may be chosen in some iterations. Results can be obtained only in the first several iterations and they cannot be improved gradually in the following steps. The accuracy of the results is also affected by noise or model errors, and the computation stops when the results fall outside their physical limits.

Acknowledgments

The work described in this paper was supported by a research grant from the Hong Kong Polytechnic University and a grant from the Hong Kong Research Grant Council project no. PolyU 5207/06E.

References

[1] Doebling, S. W., Farrar, C. R., Prime, M. B., and Schevitz, D. W., "Damage Identification and Health Monitoring of Structural and Mechanical Systems from Changes in Their Vibration Characteristics: A Literature Review,"Los Alamos National Lab., Rept. LA-13070-MS, Los Alamos, NM, 1996.

[2] Brincker, R., Andersen, P., and Cantieni, R., "Identification and Level I Damage Detection of the Z24 Highway Bridge," *Experimental Techniques*, Vol. 25, No. 6, 2001, pp. 51–57. doi:10.1111/j.1747-1567.2001.tb00047.x

[3] Maeck, J., and De Roeck, G., "Damage Assessment of a Gradually Damaged RC Beam Using Dynamic System Identification," *Proceedings of the 20th International Modal Analysis Conference*, Society of Experimental Mechanics, Bethel, CT, 4–7 Feb. 2002, pp. 1560–1566.

[4] Friswell, M. I., Mottershead, J. E., and Ahmadian, H., "Finite-Element Model Updating Using Experimental Data: Parameterization and Regularization," *Philosophical Transactions. Series A, Mathematical, Physical, and Engineering Sciences*, Vol. 359, No. 1778, 2001, pp. 169–186. doi:10.1098/rsta.2000.0719

[5] Humar, J., Bagchi, A., and Xu, H., "Performance of Vibration-Based Techniques for the Identification of Structural Damage," *Structural Health Monitoring*, Vol. 5, No. 3, 2006, pp. 215–241.

[6] Natke, H. G., "On Regularization Method Within System Identification," *Inverse Problems in Engineering Mechanics: IUTAM Symposium*, edited by M. Tanaka, and H. D. Bui, Springer, Berlin, 1993, pp. 3–20.

[7] Tikhonov, A. N., Numerical Methods for the Solution of Ill-Posed Problems, Kluwer Academic, Norwell, MA, 1995.

[8] Hansen, P. C., "Analysis of Discrete Ill-Posed Problems by Means of the L-Curve," *SIAM Review*, Vol. 34, No. 4, Dec. 1992, pp. 561–580. doi:10.1137/1034115.

[9] Hansen, P. C., "Rank-Deficient and Discrete Ill-Posed Problems," *SIAM Monographs on Mathematical Modeling and Computation*, Society for Industrial and Applied Mathematics, Philadelphia, 1998.

[10] Vogel, C. R., "Computational Methods for Inverse Problems," *Frontiers in Applied Mathematics*, Society for Industrial and Applied Mathematics, Philadelphia, 2002.

[11] Titurus, B., and Friswell, M. I., "Regularization in Model Updating," *International Journal for Numerical Methods in Engineering*, Vol. 75, No. 4, 2008, pp. 440–478. doi:10.1002/nme.2257

[12] Weber, B., Paultre, P., and Proulx, J., "Consistent Regularization of Nonlinear Model Updating for Damage Identification," *Mechanical Systems and Signal Processing*, Vol. 23, No. 6, 2009, pp. 1965–1985. doi:10.1016/j.ymssp.2008.04.011

[13] Law, S. S., and Li, X. Y., "Wavelet-Based Sensitivity Analysis of the Impulsive Response Function for Damage Detection," *Journal of Applied Mechanics*, Vol. 74, No. 2, 2007, pp. 375–377. doi:10.1115/1.2189875.

[14] Law, S. S., Li, X. Y., and Lu, Z. R., "Structural Damage Detection from Wavelet Coefficient Sensitivity with Model Errors," *Journal of Engineering Mechanics*, Vol. 132, No. 10, 2006, pp. 1077–1087. doi:10.1061/(ASCE)0733-9399(2006)132:10(1077).

[15] Newmark, N. W., "A Method of Computation for Structural Dynamics," *Journal of Engineering Mechanics Division*, Vol. 85, No. 3, 1959, pp. 67–94.

[16] Friswell, M. I., and Mottershead, J. E., *Finite Element Model Updating in Structural Dynamics*, Kluwer Academic, Norwell, MA, 1995.

[17] Dennis, J. E., and Schnabel, R. B., "Numerical Methods for Unconstrained Optimization and Nonlinear Equations," *Classics in Applied Mathematics*, Society for Industrial and Applied Mathematics, Philadelphia, 1996.

R. Kapania
Associate Editor